Available online at www.sciencedirect.com
SCIENCE DIRECT
Polymer 46 (2005) 10246–10255
polymer
www.elsevier.com/locate/polymer

Single-monomer acrylate-based resin for three-dimensional photonic crystal fabrication

Shuhui Wu*, Martin Straub, Min Gu**

Centre for Micro-Photonics and Centre for Ultrahigh-bandwidth Devices for Optical Systems (CUDOS), Faculty of Engineering and Industrial Sciences, Swinburne University of Technology, P.O. Box 218, Hawthorn, Vic. 3122, Australia

Received 31 May 2005; received in revised form 4 August 2005; accepted 10 August 2005
Available online 26 September 2005

Abstract

A single-monomer acrylate resin (SR348, Sartomer) with an aromatic ketone photoinitiator (Irgacure 369, Ciba) has been developed to produce photonic crystal structures by two-photon photopolymerisation. Compared with more complex acrylate-based resins, this one-component resin is easily prepared. The material is homogeneous before and after photocuring and has a high photosensitivity. SR348 (ethoxylated (2) bisphenol A dimethacrylate) is a difunctional monomer, which generates an insoluble crosslinked network by free radical polymerisation. The polymerised material is thermally stable up to 300 °C. Its refractive index jumps from 1.54 to 1.59 upon polymerisation. Scanning electron microscopy images of photonic crystal structures reveal a minimum structural element size of approximately 300 nm. The photonic crystals were fabricated in a 40 layer woodpile structure at a layer-spacing of 500 nm and an in-plane rod spacing of 1.5 μm. Fundamental stop gaps were observed in the stacking direction at wavelengths of 1.9–2.3 μm dependent on the rod size. Suppression of infrared light transmission of as much as 40% in the stop gap region and gap/midgap ratios of up to 0.15 demonstrate the high degree of correlation of structural elements in three dimensions.

Keywords: Photosensitive resin; Two-photon photopolymerisation; Three-dimensional microfabrication

1. Introduction

Three-dimensional (3D) polymer microstructures and, more specifically, polymer photonic crystals or photonic crystal templates generated by two-photon photopolymerisation (2PP) have found considerable interest in recent years [1–15]. As arbitrary structural arrangements can be fabricated with submicron resolution, such microstructures may facilitate numerous applications in the fields of sensors and actuators as well as optical telecommunication. For example, complex arrangements such as interconnected toothwheels assembled and driven by light have been produced [6], which demonstrate the capabilities of two-photon microstereolithography. 3D photonic crystals are a particularly interesting application of 2PP, because these periodic dielectric microstructures can be fabricated at lattice parameters small enough to observe their unusual optical properties in the near-infrared or visible spectral regions. Photonic stop bands, which suppress light propagation at certain directions or polarizations, or unusual group velocity effects, which allow for control of the direction of propagation, may be used to construct photonic devices operating at telecommunication wavelengths (1.3–1.55 μm). Importantly, a large variety of functional defects can be introduced into the photonic crystal lattice, which can be exploited for device fabrication [16].

The 2PP method is a powerful technology to generate photonic crystals. A normal one-photon photopolymerisation (1PP) process consists of the following three steps:

$$h\nu_{\mathrm{UV}} + \text{initiator} \rightarrow \text{initiator}^{\bullet}$$

$$\text{initiator}^{\bullet} + \text{monomers} \rightarrow \text{oligomers}^{\bullet}$$

$$\text{oligomers}^{\bullet} + {}^{\bullet}\text{oligomers} \rightarrow \text{polymer} \qquad (1)$$

For a 2PP process, the first step of the reaction is different:

* Corresponding authors. Tel.: +61 3 9214 4314/8776; fax: +61 3 9214 5435.
E-mail addresses: swu@swin.edu.au (S. Wu), mgu@swin.edu.au (M. Gu).

0032-3861/$ - see front matter © 2005 Elsevier Ltd. All rights reserved.
doi:10.1016/j.polymer.2005.08.030

$$2h\nu_{VIS/IR} + \text{initiator} \rightarrow \text{initiator}^{\bullet} \quad (2)$$

Instead of absorbing ultraviolet (UV) photons in a 1PP process, an initiator absorbs visible (VIS) or infrared (IR) photons in a 2PP process. Two photons are absorbed simultaneously by a photoinitiator (PI) molecule, which in its excited state turns into a radical that interacts with the surrounding monomers and triggers a polymerisation chain reaction. The reaction ceases as soon as the various oligomers generated in the process link to form the final polymer.

Typical for a nonlinear optical process, 2PP requires irradiances high enough to allow for the simultaneous absorption of two photons. Excitation beam irradiances in the order of TW/cm^2 are needed to generate a sufficiently high density of radicals with a commercial photoinitiator within a few milliseconds. Femtosecond-pulsed lasers in combination with high-numerical aperture focussing provide these irradiances. The confinement of the polymerisation reaction to the focal spot ensures the build-up of 3D microstructures, while the sample is moved along a preprogrammed pathway in three dimensions. Despite the high peak power in the focus, damage to the material can be kept to a minimum, as the resin is transparent at the fabrication laser wavelength in the visible or near-infrared part of the optical spectrum, whereas the material is strongly absorbing in the UV wavelength range.

A number of commercial resins have been available for 3D fabrication, even though a resin formulated with specific components and initiator is needed to optimise fabrication and microstructure performance. Recently, we have developed a multi-monomer based resin LN1 which has a better thermal stability than many commercial resins [11]. However, such a resin requires a complicated procedure for preparation. In this article, we demonstrate that a single-monomer acrylate-based resin with simple preparation procedure can be used to fabricate 3D photonic crystals with the 2PP method. The photonic crystals featured pronounced stop gaps in the 1.9–2.3 μm spectral range similar in shape and depth to those published earlier for the same photonic crystal arrangement fabricated with the acrylate based photopolymers SCR500 [7] and LN1 [11]. Material properties such as photosensitivity, mechanical properties, thermal stability and refractive index were investigated with LN1 as a reference material. Advantages and limitations of the SR348 resin in 3D photonic crystal fabrication were determined from the structural and spectroscopic information gained by scanning electron microscopy (SEM) and Fourier transform infrared (FTIR) spectroscopy.

2. Experiment

2.1. Materials

The resin SR348 (ethoxylated (2) bisphenol A dimethacrylate) and the LN1 components [11] were provided by Sartomer, USA. PI Irgacure 369 was purchased from Ciba, Australia. The solvents acetone and ethanol were AR grade. Refractive index liquid (n from 1.46 to 1.80) was obtained from Cargill Laboratory (USA).

2.2. Sample preparation

Resin SR348 and PI (the amount of PI varied between 1 and 4 wt% of the resin) were dissolved in acetone separately. The two solutions were mixed together and microfiltered (200 nm pore size). The solvent was removed by heating at 60–70 °C. Resin containing PI must be stored and handled in the dark. Samples for microfabrication were prepared by sandwiching a drop of resin between two glass coverslips separated by a 40 μm thick sticky-tape spacer. The sandwiched resin was fixed at a glass slide by sticky tape and inserted into the microfabrication set-up. Preparation of the photopolymer LN1 is described elsewhere [11].

2.3. Photodifferential scanning calorimetry (PhotoDSC)

A TA-Instruments Photo-DSC Q1000 was used to monitor the photopolymerisation process. A 100 W high pressure mercury arc lamp was used as light source with spectral range 250–650 nm. The experiment was performed under nitrogen atmosphere at 30 °C, using a light intensity of 20 mW/cm^2. Light was turned on after 0.5 min at the desired temperature. About 10 mg of the SR348 and LN1 resins were used containing 4 wt% PI. The heat (W/g) produced during polymerisation was recorded as a function of the reaction time (min).

2.4. Dynamic mechanical analysis (DMA)

DMA was conducted on a Perkin–Elmer Pyris Series-DMA7 in the three point bending mode. UV-cured SR348 and LN1 resin samples with 2 wt% PI were prepared at a size of $25 \times 10 \times 1$ mm^3 (length, width, height). The temperature was varied from −30 to 150 °C at a speed of 2 K/min. A static force of 220 mN was applied to the sample, as well as a dynamic force of 200 mN at a frequency of 1 Hz. The sample was subjected to nitrogen gas at a flow rate of 40 mL/min. The result was shown as storage modulus, loss modulus as well as tanδ (ratio of loss modulus to storage modulus) versus temperature.

2.5. Thermal stability

The thermal stability of the materials was investigated by thermal gravimetric analysis (TGA). About 30 mg of the fully cured resins SR348 and LN1 with 2 wt% PI were used in this measurement. TA-Instruments Q500 TGA was used under nitrogen atmosphere at a flow rate of 50 mL/min. The temperature was ramped from room temperature to 800 °C at a speed of 20 K/min. The result was presented as weight

fraction (of original sample weight) versus temperature curve.

2.6. Refractive index measurement

The refractive index of a particle was measured by using the so-called Becke line method [17]. The Becke line is a bright halo of light that appears around the perimeter of a particle if the refractive indices of the particle and surrounding medium are different. It is caused by the concentration of refracted light rays along the edge of the particle. When the sample leaves the focal plane moving away from the objective, the Becke line moves towards the region with higher refractive index. The Becke line disappears if there is no refractive index mismatch. By choosing a proper refractive index matching liquid, the Becke line effect can be minimized, and the refractive index of the particle can be approximated by that of the matching liquid. The refractive index liquids were supplied by Cargill Laboratory with resolution of 0.01, their refractive index ranging from 1.46 to 1.80.

2.7. Fabrication

The microfabrication set-up is described in detail elsewhere [7]. An ultrashort-pulsed visible light beam at a wavelength of 580 nm from a 76-MHz repetition-rate femtosecond-pulsed Ti:sapphire laser combined with an optical parametric oscillator with intra-cavity frequency doubler (Mira 900-F and Mira OPO, Coherent, Santa Clara, CA, USA) was focussed into the liquid resin by a numerical aperture (NA) 1.4 objective to initiate polymerisation.

Microstructures were built up layer-by-layer by moving the sample with a 3D piezoelectric scanning stage at a scan speed of 60 μm/s. A frame was fabricated about the photonic crystal structures in order to stabilize them laterally. The focal radiant flux was chosen as 0.56, 0.52, 0.40, 0.30 and 0.17 mW to fabricate sample A, B, C, D and E, respectively. After fabrication, the remaining liquid material was washed away by rinsing the coverslips in pure ethanol.

2.8. Scanning electron microscopy (SEM)

The coverslip with the five samples was coated with a few nanometers of carbon and gold before imaging. A JEOL JSM-840 scanning electron microscopy with an acceleration voltage of 10 kV was used to resolve details of the microstructures fabricated with SR348 resin (probe current 0.6 nA).

2.9. Fourier-transform infrared (FTIR) spectroscopy

Photonic bandgaps were measured using a Nicolet Nexus FTIR spectrometer combined with a Continuum infrared microscope (MCT detector, XT-KBr beamsplitter, 32× NA 0.65 objective and condenser, 200 scans in transmission at 4 cm^{-1} resolution). In addition to showing them as measured, spectra were baseline-corrected for scattering effects arising from the various Bragg planes in the samples as well as from imperfections.

3. Results and discussion

3.1. Material

Bulk-like 3D microstructures such as a bull sculpture from urethane acrylate SCR500 [4], or more recently a Venus torso [12] and a Sydney Opera House micromodel [9] from inorganic–organic hybrid materials, are fabricated with relative ease. By contrast, structures with isolated or only weekly linked structural elements such as photonic crystals featuring rods with diameter of order of 200 nm [7–12] are a challenge for the 2PP technique. For such structures choice of the right material is crucial. Microstructures need to be mechanically stable and free from distortions related to shrinkage during the polymerisation process. Postprocessing of the samples such as removal of resin which is not polymerised must leave the fabricated structures unharmed. The resin must be homogeneous and transparent at the fabrication wavelength. Ideally, it should have a refractive index close to that of glass ($n \approx 1.5$) in order to focus the fabrication beam deeply into it without degrading the focal spot too much by aberrations. For optical microstructures such as photonic crystals the polymerized material must be transparent at the operational wavelength such as certain telecommunication wavelengths in the near-infrared spectral region. In addition, high thermal stability is desired if, for example, conversion of a polymer template into a high dielectric contrast structure requires filling of the polymer microstructure at elevated temperatures.

The various materials used in recent years for 2PP satisfy these criteria to a different extent. Early experiments were performed with resins from commercial suppliers. Examples of such resins with unchangeable composition are Nopcocure 800 [3,5] and Norland NOA63 [6], which are free-radical polymerisation systems. The minimum structural element size of the Nopcocure structures was 1.0 μm, and the Norland NOA63 structures were at most 5 μm in total size with approximately 500 nm thick elements. However, high-quality structures with only modest distortions by shrinkage have been generated by MicroChem's SU-8 [8,10] with structural element diameters down to 180 nm [10]. The commercially available polysiloxane polymer inorganic polymer glass (IPG, RPO Inc.) allowed for a minimum size of isolated structural elements of approximately 350 nm [9], but the quality of the photonic crystals was degraded significantly as a result of shrinkage. To overcome the limitations of commercial resins pure acrylate-based polymers SCR500 [4,7] (developed by Japan

Synthetic Rubber Company, but not commercially available) and LN1 [11] as well as inorganic–organic hybrid polymers [8] were developed to meet specific requirements. Isolated polymerised voxels with a diameter of merely 120 nm were fabricated [4,8]. Comparing photonic crystals with near-IR stop bands, the structures from the pure polymer material [7,11] revealed more pronounced stop gap features than those fabricated by the Ormocer hybrid material [8]. Apparently, the loss of correlation of structural elements in three-dimensions due to material shrinkage is more serious for the hybrid materials used so far. However, the Ormocers are known to have better optical transparency at telecommunication wavelengths. Both pure photopolymers and hybrid materials can be developed to adopt specific refractive index values.

Regarding the chemical processes involved, SCR 500 [4,7], Nopcocure 800 [3,5], IPG [9] and Ormocers [8,12] rely on free radical polymerisation, which transforms the material from a liquid into a solid during the laser beam exposure. In contrast, SU-8 is crosslinked in two steps: formation of a strong acid during the exposure process followed by acid-initiated, thermally driven epoxy crosslinking during the post exposure bake step.

Naturally, a resin formulated with specific components and initiators more easily optimises fabrication and microstructure performance. To this end, the acrylate-based resin LN1 was developed in our group [11]. It contains eight components of multi-functional monomers and oligomers, which are mixed before the initiator is added. Due to the high viscosity of its components, it is difficult to weigh, and it may take a few days to complete the mixing procedure. The resin must be kept in a sealed container to prevent its volatile low-boiling point components from evaporation. In order to simplify the preparation procedure, to make preparations better reproducible, and also to increase the shelf-life of the resin, a single monomer resin consisting of SR348 (ethoxylated (2) bisphenol A dimethacrylate, Sartomer, Scheme 1) is used in this work to fabricate 3D microstructures.

SR348 is a difunctional monomer, the functional groups of which are located at both ends of the molecule generating an insoluble crosslinked network by free radical polymerisation. The aromatic ketone Irgacure 369 (Ciba) was used as a PI. The un-reacted monomer has a good solubility in ethanol allowing the resin outside the polymerised microstructure to be washed away without harming the structure. As the two functional groups are located at end of the long rigid molecule, shrinkage after polymerisation is expected to be low. Moreover, the one-component resin is homogeneous, and its refractive index of 1.54 is suitable for high numerical aperture focusing.

Table 1 summarizes the polymerisation process, preparation and post-processing of the most common resins used in recent years for two-photon microfabrication of photonic crystals. The minimum structural element size achieved with the various resins, the shortest photonic stop band wavelength, as well as the bandgap-induced attenuation of infrared light per layer of woodpile structure are listed as key performance indicators of the photonic crystals in the right columns.

3.2. Photosensitivity

The curing process of SR348 and LN1 was monitored by PhotoDSC at the same temperature (30 °C), the same photoinitiator concentration (4 wt%) and the same light irradiance (20 mW/cm^2). PhotoDSC measures the polymerisation efficiency of the resins during light exposure, as the shape of the polymerisation peak demonstrates their photosensitivity. Fig. 1 presents the heat flow (W/g) versus time (min) for SR348 and LN1. The peak of SR348 is much sharper than that of LN1, indicating that SR348 has a higher photosensitivity than LN1. A high photosensitivity is required to polymerise the material by 2PP at a reasonable speed. The resin is polymerised as soon as the density of radicals exceeds a certain minimum concentration, which is the threshold of photopolymerisation. For the same initiator, this value is independent of the particular process that leads to generation of radicals and should be the same for 1PP and 2PP. A possible way to increase the photosensitivity is to use a more efficient PI. Such initiators have a large two-photon absorption cross-section, with chromophores normally having π-conjugation and high planarity [18,19]. It should also have a fast photogeneration rate to produce free radicals, leading to activation of chemical functionality [2,20,21]. Design and synthesis of efficient two-photon PI is a novel research direction for photonic applications. The SR348 resin still has potential to improve its photosensitivity with this new generation of two-photon initiators, and to reduce the polymerisation threshold. Beyond the threshold, the polymerised volume depends on laser power and irradiation time [12], its shape being related to the two-photon point-spread function [7].

Nevertheless, the resins SR348 and LN1 allow for efficient fabrication of microstructures using the commercially available photoinitiator Irgacure 369. Initiators with a different absorption range can be used if fabrication is performed at different wavelengths. In most cases,

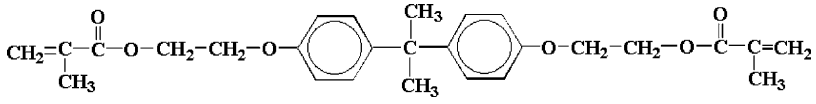

Scheme 1. Structure of SR348. Ethoxylated (2) bisphenol A dimethacrylate is a difunctional monomer. The end groups of the long, rigid molecule become crosslinked as soon as free radical polymerisation is triggered by a photoinitiator.

Table 1
Polymerisation mechanism, preparation and post-processing of the SR348 resin compared to selected other resins used for two-photon microfabrication. Minimum structural element size, shortest photonic bandgap wavelength and maximum suppression of light transmission of related woodpile-type photonic crystals are listed in the right columns.

Resin	Type of material	Polymerisation process	Preparation	Post-processing	Minimum structural element size (nm)	Bandgap (μm)/max. suppression of transmission (% per layer)
SU-8	Epoxy resin	(1) Acid formation during exposure (2) Acid-initiated crosslinking during post-bake	Commercial resin (Micro-Chem), no further preparation	(1) Post-bake (2) Washout in special developer	180 [10] (photonic crystal)	1.3/3.0
SCR500	Urethane acrylate polymer	Free radical polymerisation	Commercial supplier (Japan Synthetic Rubber Co., limited customers)	Washout in ethanol	200 [7] (photonic crystal), 120 [4] (isolated voxels)	1.5/1.7
Ormocer	Inorganic–organic hybrid polymer	Free radical induced cross-linking of organic groups attached to inorganic back-bone	Custom-made [8,12], but also commercially available (micro resist technologies)	(1) Washout by 4-methyl-2-pentanone (2) UV post-curing Washout by toluena	200 (photonic crystal), 120 [12] (isolated voxels)	1.2/0.8 [8] (without stabilization by frame)
IPG	Inorganic polymer glass (inorganic–organic polysiloxane polymer)	Free radical induced cross-linking of organic groups attached to polysiloxane backbone	Photoinitiator is added to commercial resin (RPO Inc.)		350 [9] (photonic crystal)	4.2/1.1
LN1	Urethane acrylate polymer	Free radical polymerisation	(1) Eight components (Sartomer) are mixed (2) Photoinitiator is added	Washout by ethanol	$<$200 [11] (photonic crystal)	2.3/1.3
SR348	Ethoxylated (2) bisphenol A dimethacrylate polymer	Free radical induced cross-linking of acrylate end groups	Photoinitiator is added to commercially available SR348 monomers (Sartomer)	Washoutby ethanol	300 (photonic crystal)	1.9/1.3

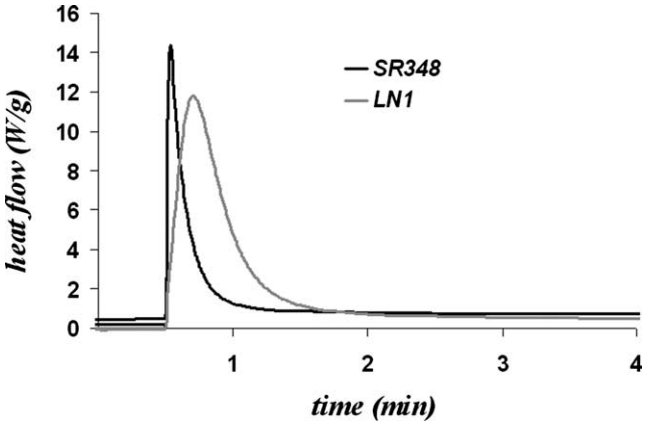

Fig. 1. Photopolymerisation process of SR348 and LN1 monitored by PhotoDSC. The onset and progress of the cure for the single-monomer resin SR348 are much faster than for the multi-component resin LN1, demonstrating the high photosensitivity of the SR348 resin.

commercial resins have no such flexibility to choose an initiator.

3.3. Mechanical properties

Thermal mechanical properties are important for the resin performance, although limited information is available for commercial resins. Because polymerisation is a dynamic process, the mechanical properties can vary at its different stages. In order to simplify the measurement, cured resin SR348 and LN1 was used. The thermal mechanical properties (Fig. 2) were investigated by dynamic mechanical analysis. SR348 has a lower storage modulus at low

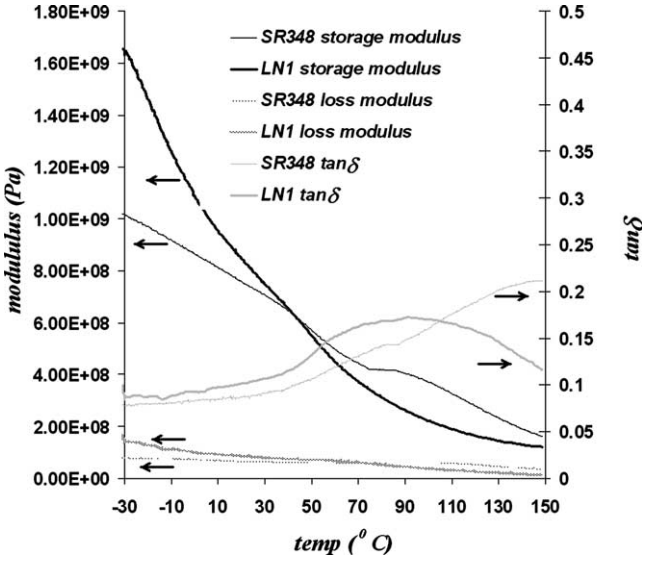

Fig. 2. Dynamic mechanical properties of SR348 and LN1. With its high storage modulus, the cured multi-component resin LN1 is more rigid at low temperatures than SR348. The maximum of its tan δ curve at 95 °C indicates a distinguished glass transition temperature, whereas for the cured SR348 the glass transition is either outside the measurement range or is suppressed by the high level of crosslinking in the material.

temperatures compared with cured LN1. However, the storage modulus of LN1 drops faster with increasing temperature. Both materials have a similar modulus value around 44 °C, but SR348 is more stable at higher temperatures with properties changing less rapidly during thermal change. A plateau starts to appear in the LN1 storage modulus curve beyond 90 °C due to material transfer from glass state to rubber state with increasing temperature. No such plateau appears in the SR348 curve. Instead, a small step-wise change is observed around 80–90 °C.

The maximum value of tan δ can be used to determine the glass transition temperature T_g. For a multi-component resin, curing may turn the homogeneous blend into a multiphase system, because the increase in the molecular weight causes a decrease in configurational entropy of mixing as the cure proceeds, finally resulting in multiple values of T_g. A single peak at about 100 °C in the LN1 tan δ curve demonstrates that LN1 has one distinguished glass transition point, which corresponds to the onset of the plateau in the storage modulus curve. Apparently, all of the eight components make up a homogeneous phase at the molecular level after curing. The broadening of the glass-to-rubber transition region is due to superposition of movements of different multi-components. The polymer may have a broader distribution in molecular weight, being composed of an insoluble network as well as some low molecular weight components and less crosslinked copolymer [22]. Different monomers react at different speed under light expose. Therefore, the composition of the copolymer varies from the beginning to the end as the cure proceeds.

By contrast, no peak is observed in the SR348 tan δ curve. This may be explained by two possible reasons: (1) The measured temperature has not yet reached the glass transition temperature of SR348. The thermal stability of the material (see below) limits the measurement range to under 200 °C. (2) The peak is diminished because of the extremely high level of crosslinking [22]. Reason (1) indicates that SR348 is a hard glass-state material. Its T_g value is also not detected in the DSC curve (figure not shown here). Although T_g has not been determined, SR348 is truly a hard fragile material. The molecular formula in Scheme 1 also provides the information about this nature of the material. Reason (2) indicates that this material is crosslinked uniformly (single phase, homogeneous composition of polymer) throughout the solidification process in a network of high crosslinking density.

No matter which reason is correct, both one-component and multi-component resins have their advantages. One-component polymers are easy to prepare and homogeneous throughout the polymerisation process. They can have properties suitable for fabrication and structure performance such as high photosensitivity and refractive index (see below). On the other hand, miscible components may be introduced into the resin to increase flexibility and toughness of the material, although this may be at the expense of the performance of the other components.

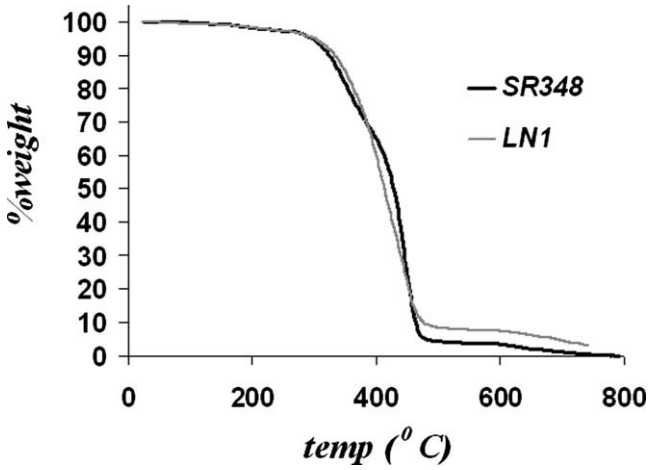

Fig. 3. TGA curves of cured SR348 and LN1. Both the cured single-monomer resin SR348 and the multi-component resin LN1 decay rapidly beyond 300 °C.

Clearly, the optimum formulation of the composition depends on the specific requirements of microstructure fabrication and application.

3.4. Thermal stability

Fig. 3 shows that both SR348 and LN1 have similar thermal stability. They start to decompose at about 200 °C with a rapid drop beyond 300 °C, and the decomposition process is almost completed at about 500 °C.

3.5. Refractive index

The refractive index of the resins before curing is provided by the supplier. For the cured samples it was measured by the Becke line method [17]. The refractive index of LN1 before curing is 1.49 (averaged over the eight components of the LN1 resin), and it changes to 1.53 after curing. For SR348, the value jumps from 1.54 to 1.59 by

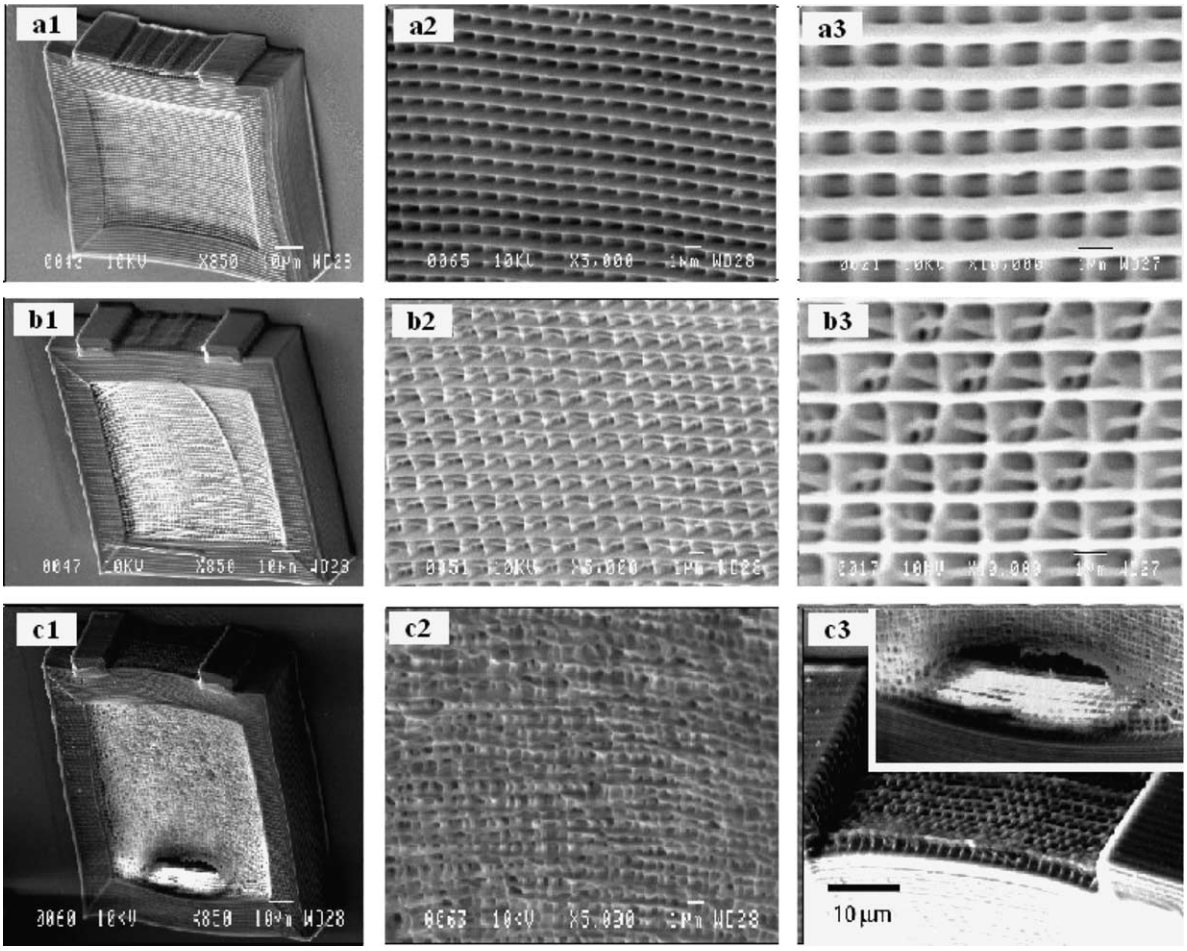

Fig. 4. Scanning electron microscope images of 3D photonic crystals fabricated from the SR348 single-monomer resin by 2PP. The photonic crystals were stacked in a woodpile structure arrangement surrounded by a frame (samples A, B, D in order of decreasing rod size). A patch of crystal structure was fabricated outside the frame between two pillars to investigate the rod cross-section. Sample A: (a1) complete microstructure, (a2) magnified section of the crystal surface, side view at 40° tilt angle; (a3) top view at high magnification. Sample B: (b1)–(b3) images recorded under the same condition as sample A. Sample D: (c1) complete microstructure, (c2) magnified section of the crystal surface, side view at 40° tilt angle; (c3) The patch of the woodpile structure fabricated outside the frame and the rift near the frame at the bottom of sample D (inset, magnified image) demonstrate the structural arrangement in the third dimension.

polymerisation. Apparently, before curing both materials have a refractive index near 1.5, which allows to focus deeply into the resin and to fabricate microstructures at sufficiently large vertical dimensions, but the refractive index mismatch is smaller for LN1. Cured SR348 has a higher refractive index value than LN1. Thus, it provides the polymerised photonic crystals with a slightly higher dielectric contrast, thereby improving their bandgap properties.

3.6. SEM images

Fig. 4 shows SEM images of photonic crystals, which were fabricated by 2PP of the SR348 (samples A, B, D, see Section 2). Woodpile structures were stacked layer-by-layer with a layer spacing of 500 nm and an in-plane rod spacing of 1.5 μm. The structures consist of 40 layers with rods in adjacent layers oriented perpendicular to each other and second-nearest layers displaced by half an in-plane period (i.e. 750 nm) relative to each other. A 15 μm wide frame was fabricated before the photonic crystal structure is scanned to stabilize the 65×70 μm-woodpile structure in-plane. In order to check the quality of the structural arrangement in the third dimension and to characterize the rods in the vertical direction, on one side the photonic crystal structure was extended outside the frame by a few rows of rods held between two pillars.

Sample A, which was fabricated at the highest focal radiant flux of 0.56 mW, is seen at a tilt angle of 40° (Fig. 4(a1), ×850, scale bar 10 μm; (a2), ×5000, scale bar 1 μm). In addition, a top-view image was recorded at high magnification to determine the lateral rod dimensions (Fig. 4(a3), ×10000, black scale bar 1 μm). It reveals the

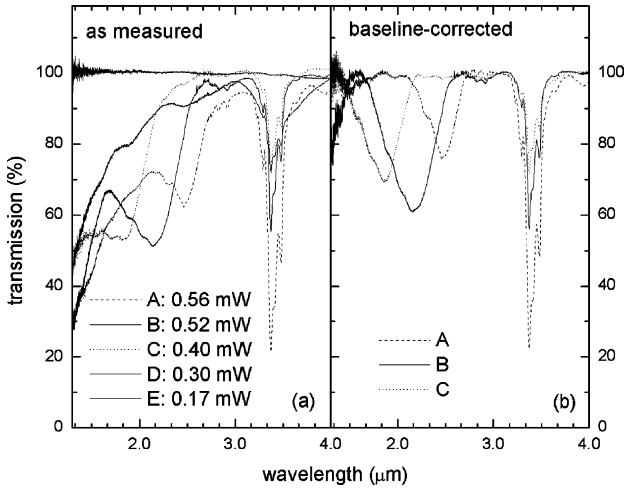

Fig. 5. FTIR spectra of woodpile-type photonic crystals measured in the stacking direction. (a) Spectra of samples A–E as measured, (b) spectra of samples A–C after baseline-correction for scattering effects revealing pronounced photonic stop gaps in the 1.9–2.3 μm range. The stop bands shift to shorter wavelengths on reduction of the rod cross-section. Sample D (broken) and sample E (empty) do not show signatures of photonic stop gaps.

three topmost layers, the second and third layer being increasingly out of focus. The high fabrication beam intensity resulted in thick rods of a lateral diameter of approximately 690 nm and an axial (i.e. vertical, in the focussing direction) diameter of roughly 1.4 μm ensuring a stable and strongly interconnected structural arrangement. The focal spot of an objective of NA 1.4 is approximately three times larger in the axial direction compared to the lateral direction, whereas the observed elongation of the rods in the vertical direction was only by about a factor of two. However, for sample A the patch of the photonic crystal structure outside the frame did not allow for a precise determination of the border of the rods due to their strong overlap. The large vertical stripes in the patch of crystal outside the frame as seen in the upper part of Fig. 4(a1) are due to bundles of rods fabricated at different scan directions. Note also that the frame is bent inwards by the strong forces acting in the process of material shrinkage during polymerisation. Shrinkage is an intrinsic property of the polymerisation process due to bond variations and cohesive energy density changes. When a covalent bond is formed between two monomer molecules, the distance between them is approximately half as much as that between two molecules experiencing van der Waal's force [23]. Moreover, it should be mentioned that for focal intensities higher than the fabrication beam intensity of sample A, rods start to overlap in-plane and the material turns into a bulk solid. The photonic crystal structure B, which features the most pronounced photonic band gap (see below), was imaged under the same conditions as sample A (Fig. 4(b1)–(b3)). Due to its lower fabrication beam intensity it consists of rods with a lateral diameter of only 340 nm and an axial diameter of 870 nm. Therefore, the rectangular frame holding them in place does not show strong distortions. The woodpile structure corresponds well to its design, although it is contracted considerably in the vertical direction. Moreover, deviations from ideal straight lines due to shrinkage are seen in the magnified image Fig. 4(b3), which resolves the topmost four layers of the structure. The big vertical line in the upper right part of the crystal surface is from debris which got stuck during the wash-out process.

Further reduction of the focal intensity results in increasingly unstable structures. Sample C (not shown), which still reveals a photonic stop band (see below), is characterized by strong distortions of the rods in-plane as well as a strong vertical contraction of the woodpile structure. In sample D (Fig. 4(c1)–(c3)), which was fabricated at even lower radiant flux, the rods were too weak to establish the woodpile structure and were torn apart by the shrinkage opening a rift at the lower part of the frame. As a result, the structure contracted not only vertically but also in-plane, and not much space was left between the rods. The lateral rod diameter in samples C and D was approximately 300 nm, which means that further reduction of the fabrication radiant flux mainly weakened the rods without reducing their size substantially. Most likely, the

SR348 was only partially crosslinked in samples C and D resulting in a deviation of the viscoelastic properties from those of the fully cured material. Deformation of structural elements under stress due to shrinkage can then occur more easily resulting in an unstable network, which however may consume a similar volume. The axial size of the rods also remained largely unchanged and amounted to 800–950 nm in samples C and D (Fig. 4(c3), ×3000). It appears that the observed lateral diameter of about 300 nm is the minimum structural element size, which can be achieved with the SR348 resin. Therefore, miniaturization of the microstructures is limited to this resolution. In addition to providing information on the rod dimensions Fig. 4(c3) demonstrates the well-defined forty-layer woodpile arrangement of our photonic crystals even though in sample D the rods in the outside-patch of the crystal were truncated during the washout. The inset which is a magnified image of the rift located on its frame bottom again shows the regular layer-by-layer arrangement of the structure. Finally, it should be noted that in sample E (not shown) the rods were entirely washed away when the sample was rinsed with the washout solvent after the laser microfabrication was completed.

3.7. FTIR spectra

Fourier transform infrared (FTIR) spectra in the 1–4 μm spectral range were recorded in transmission in the stacking direction of the woodpile structures. Fig. 5 shows the infrared spectra for all of the samples A–E as measured (a) as well as the baseline-corrected spectra of samples A–C, which feature pronounced photonic stop bands (b). Sample E, in which no photonic crystal structure was left inside the frame, generates a flat 100%-line in the FTIR spectrum. It demonstrates the high signal-to-noise ratio of the spectrometer and gives evidence that the infrared beam did not penetrate the frame. The decreasing depth of the polymer absorption bands in the 3.2–3.6 μm range from sample A to C reflects the reduction of the rod size with smaller fabrication intensity. The similar depth of the absorption bands for samples C and D further demonstrates that the rod dimensions do not change any more at the lowest intensities. For all of the samples A–D a strong drop in the infrared transmission to short wavelengths is observed due to scattering of light by the manifold of Bragg planes as well as imperfections in the sample. Superimposed on this drop are pronounced dips in the transmission at 2.3 μm for sample A, 2.1 μm for sample B, and 1.9 μm for sample C, which signify the photonic stop gaps in these structures. In order to eliminate the influence of scattering and to investigate the shape of the dips in detail, a baseline correction was performed with the spectra of sample A–C, the result of which is seen in Fig. 5(b). The depth of the stop gap features varies from sample A to C with sample B allowing for a suppression of infrared light transmission of as much as 39%. For sample A a suppression of transmission by 24% and sample C by 31% was observed. The gap shape is almost identical for the three samples showing a characteristic shoulder at the short wavelength edge, similar to what was observed with the urethane acrylate resins SCR500 [7] and LN1 [11]. The depth of the gap as well as its gap/midgap ratio of 0.15 are close to the values measured for the corresponding structure for LN1 [11], which suppressed infrared transmission by 40% at the midgap wavelength of 2.3 μm with a gap/midgap ratio of 0.13. However, computer-simulations of the dependence of spectral features on structural details, which are outside the scope of this article, are required to explain the precise gap shape. The smaller depth of the stop band features for samples A and C compared to sample B can be explained by the high filling ratio (dielectric/air volume) of sample A and the increasing structural imperfection of sample C, consistent with our earlier experiments on photopolymerised photonic crystals [7, 11]. Sample B reveals a higher-order stop gap at 1.4 μm, which demonstrates the high degree of internal correlation of structural elements, again similar to the observations with the resins SCR500 and LN1. The maximum suppression of infrared light transmission of 39% in the stacking direction of the stabilized woodpile structure corresponds to an attenuation of 1.3% per layer of the structure. The right column of Table 1 compares the attenuation achieved in similar woodpile structure arrangements, which except of the Ormocer structure were all stabilized by a frame running parallel/perpendicular to the rods. While SCR500 and SU-8 structures revealed a higher attenuation per layer than the SR348 crystals, for the IPG and Ormocer structures lower values were measured.

4. Conclusions

The single-monomer resin SR348 allows for the fabrication of photonic crystal structures with submicrometer resolution of structural elements by 2PP featuring bandgaps in the near-infrared spectral region. Compared with other resins, SR348 is easy to prepare and remains homogeneous throughout the polymerisation process. The type of photoinitiator and its loading can be chosen to optimise the fabrication procedure and to obtain the best microstructure performance.

The difunctional acrylate resin SR348 polymerises into an insoluble network. The SR348 resin has a higher photosensitivity and a slightly higher refractive index than the eight component resin LN1, both resins containing the aromatic ketone Irgacure 369 as PI. Thermal gravimetric analysis demonstrates disintegration of the cured photopolymer above 300 °C. Dynamic mechanical analysis does not determine the glass transition temperature of SR348, contrary to the LN1 resin which has a broad glass to rubber

transition region and a single distinguished T_g value of approximately 95 °C. Additional miscible components need to be added to the SR348 to improve its flexibility and toughness.

For photonic crystal applications a small minimum structural element size, a short photonic bandgap wavelength, and a high suppression of light transmission in the bandgap region are the key performance indicators. Forty-layer woodpile structures with a minimum lateral rod diameter of 300 nm were fabricated at a layer distance of 500 nm and an in-plane rod spacing of 1.5 μm. FTIR spectroscopy revealed photonic stop gaps about the stacking direction in the 1.9–2.3 μm wavelength range with suppression of infrared transmission of as much as 40% and a gap/midgap ratio of up to 0.15 consistent with results of LN1 but not reaching the shorter gap wavelengths of SU-8 and Ormocer structures or the high attenuation in the SU-8 samples. With SR348, fabrication at the lowest intensities did not result in a reduction of the structural element size to below 300 nm. Instead, structures became increasingly unstable with strong distortions due to polymer shrinkage. Applications of the SR348 monomer resin in 2PP with standard high numerical aperture focussing are limited to this resolution of structural elements. In conclusion, the SEM images as well as the FTIR spectra demonstrate that in a limited range of fabrication beam intensities photonic crystal structures can be fabricated with structural elements small enough for bandgaps in the near-IR spectral region. Higher intensities result in a too high filling ratio or even polymerise the material completely, whereas lower intensities result in weak structures which cannot sustain deformation due to shrinkage. Other miscible components need to be introduced into the formula to improve the viscoelastic properties of the material and to improve the resolution further.

Acknowledgements

We acknowledge that Prof Robert Shanks at RMIT, Australia, kindly helped us to carry out the DMA measurements and discussed the results. This work was produced with the assistance of the Australian Research Council under the ARC Centres of Excellence program. CUDOS (the Centre for Ultrahigh-bandwidth Devices for Optical Systems) is an ARC Centre of Excellence.

References

[1] Maruo S, Nakamura O, Kawata S. Opt Lett 1997;22(1):132.
[2] Cumpston BH, Ananthavel SP, Barlow S, Dyer DL, Ehrlich JE, Erskine LL, et al. Nature 1999;398:51.
[3] Sun HB, Kawakami T, Xu Y, Ye JY, Matuso S, Misawa H, et al. Opt Lett 2000;25(15):1110.
[4] Kawata S, Sun HB, Tanaka T, Takada K. Nature 2001;412:697.
[5] Sun HB, Matsuo S, Misawa H. Appl Phys Lett 1999;74(6):786.
[6] Galajda P, Ormos P. Appl Phys Lett 2001;78(1):249.
[7] Straub M, Gu M. Opt Lett 2002;27(20):1824.
[8] Serbin J, Ovsianikov A, Chichkov B. Opt Express 2004;12(21):5221.
[9] Straub M, Nguyen LH, Fazlic A, Gu M. Opt Mater 2004;27(3):359.
[10] Deubel M, Von Freymann G, Wegener M, Pereira S, Busch K, Soukoulis CM. Nat Mater 2004;3:444.
[11] Nguyen LH, Straub M, Gu M. Adv Funct Mater 2005;15(2):209.
[12] Serbin J, Egbert A, Ostendorf A, Chichkov B, Houbertz R, Domann G, et al. Opt Lett 2003;28(5):301.
[13] Maruo S, Ikuta K, Korogi H. Appl Phys Lett 2003;82(1):1.
[14] Kim JM, Muramatsu H. Nano Lett 2005;5:309.
[15] Seet KK, Mizeikis V, Matsuo S, Juodkazis S, Misawa H. Adv Mater 2005;17(5):541.
[16] Joannopoulos J, Meade R, Winn J. Photonic crystals. New York: Princeton University Press; 1995.
[17] Faust RC. Proc Phys Soc 1955;B68:1081.
[18] Zhou W, Kuebler SM, Braun KL, Yu T, Cammack JK, Ober CK, et al. Science 2002;296:1106.
[19] Lin TC, Chung SJ, Kim KS, Wang XP, He GS, Swiatkiewicz J, et al. Adv Polym Sci 2003;161:157.
[20] Belfield KD, Ren XB, Van Stryland EW, Hagan DJ, Dubikovsky V, Miesak EJ. J Am Chem Soc 2000;122:1217.
[21] Rumi M, Ehrlich JE, Heikal AA, Perry JW, Barlow S, Hu Z, et al. J Am Chem Soc 2000;122:9500.
[22] Ferry JD. Viscoelastic properties of polymers. New York: Wiley; 1980.
[23] Cai Y, Jessop JLP. Photopolymerization, free radical. Part 3. Monomers. Encyclopedia of polymer science and technology. New York: Wiley; 2003 [Article online www.mrw.interscience.wiley.com/epst/articles/pst490/bibliographyfs.html].